Parametric sensitivity analysis of fast load changes of a dynamic MCFC model

K. Sternberg K. Chudej H.J. Pesch

A. Rund

This article is a preprint. It was published in Journal of Fuel Cell Science and Technology by American Society of Mechanical Engineers (ASME). The version of record is available at http://dx.doi.org/10.1115/1.2885400.

Parametric Sensitivity Analysis of Fast Load Changes of a Dynamic MCFC Model

K. Sternberg, K. Chudej, H.J. Pesch, and A. Rund

Universität Bayreuth, Lehrstuhl für Ingenieurmathematik, 95440 Bayreuth, Germany

Summary. Molten carbonate fuel cells are well suited for stationary power production and heat supply. In order to enhance service life time, hot spots, resp. high temperature gradients inside the fuel cell have to be avoided. In conflict with that, there is the desire to achieve faster load changes while temperature gradients stay small. For the first time, optimal fast load changes have been computed numerically, including a parametric sensitivity analysis, based on a mathematical model of Heidebrecht. The mathematical model allows for the calculation of the dynamical behavior of molar fractions, molar flow densities, temperatures in gas phases, temperature in solid phase, cell voltage, and current density distribution. The dimensionless model is based on the description of physical phenomena. The numerical procedure is based on a method of lines approach via spatial discretization and the solution of the resulting very large scale optimal control problem s.t. a differential-algebraic equation system by a nonlinear programming approach.

Keywords: molten carbonate fuel cell, load changes, optimal control, parametric sensitivity analysis.

1 Dynamic 2D crossflow model of a molten carbonate fuel cell

A detailed dynamic 2D crossflow model of a molten carbonate fuel cell (MCFC) due to our co-operation partners Heidebrecht and Sundmacher [1, 2] in a project financed by the German Ministry for Education and Research is used for the numerical computation of fast load changes by optimal control [3]. The mathematical model allows for the calculation of the dynamical behavior of molar fractions, molar flow densities, temperatures in gas phases, temperature in solid phase, cell voltage, and current density distribution. The dimensionless model is based on the description of physical phenomena. Numerical simulation results for the model can be found in [1, 2, 4]. The model represents all variables of a general MCFC in dimensionless form. A closely related variant of the model was recently validated for a real MCFC, a HotModule [5] produced by the project partner CFC Solutions GmbH, Munich, and operated by another project partner, IPF Heizkraftwerksbetriebsges. mbH, Magdeburg, see [6].

Main assumptions of the model are isobaric conditions, e.g. no pressure drops across the gas channels, and one-dimensional plug flow conditions in the anode and cathode gas phase. Three different currents and current densities are used in the layers of the solid. For a detailed description and technical discussion including all the modeling assumptions we refer to [1, 2]. In Fig. 1, a compartment model is given together with the relevant mathematical variables. For simplicity, almost the same notation is used as in [1, 2]. Spatial domain is $\Omega = [0,1] \times [0,1]$ with spatial coordinates ζ_1 and ζ_2. Time is denoted by τ. The index i refers to the different chemical substances: $i \in \mathcal{I}$:={CH_4, H_2O, H_2, CO, CO_2, O_2, N_2}. Fig1

[0] Corresponding Author: Kurt Chudej, e-mail: kurt.chudej@uni-bayreuth.de

1.1 Mathematical variables and equations

For given or controlled input parameters, the numerical solution of the dynamic model predicts the behaviour of the states, which fulfill a coupled partial and ordinary differential-algebraic equation system.

The *input parameters* are:

- Cell current $I_{\mathrm{cell}}(\tau)$.
- At the inlet of the anode gas channel: molar fractions $\chi_{i,\mathrm{a,in}}(\tau)$, gas temperature $\vartheta_{\mathrm{a,in}}(\tau)$, and molar flow density $\gamma_{\mathrm{a,in}}(\tau)$.
  Abbreviation: $w_{\mathrm{a,in}}(\tau) = ((\chi_{i,\mathrm{a,in}})_{i\in\mathcal{I}}, \vartheta_{\mathrm{a,in}})$.
- At the inlet of the catalytic combustor: Gas temperature $\vartheta_{\mathrm{air}}(\tau)$, air number $\lambda_{\mathrm{air}}(\tau)$.
- Switch for cathode recycle: $R_{\mathrm{back}}(\tau) \in [0,1]$.

In this paper we choose $u(\tau) := \gamma_{\mathrm{a,in}}(\tau)$ as a scalar boundary control, a selection that is technologically feasible and will be used in Sect. 2.

The following *states* appear in the model equations (1-14):

- In the anode gas channel ($j = \mathrm{a}$) resp. the cathode gas channel ($j = \mathrm{c}$): molar fractions $\chi_{i,j}(\zeta,\tau)$, gas temperatures $\vartheta_j(\zeta,\tau)$, and molar flow densities $\gamma_j(\zeta,\tau)$. Near the electrodes: partial pressures $\varphi_{i,j}(\zeta,\tau)$. Note that a subset of the chemical substances, i.e. for the molar fractions and partial pressures, is sufficient for the numerical solution.
  Abbreviation: $w_j(\zeta,\tau) := ((\chi_{i,j})_{i\in\mathcal{I}}, \vartheta_j)$, $w_{\mathrm{a|c}} := (w_{\mathrm{a}}, w_{\mathrm{c}})$.
- In the solid (electrolyte): temperature $\vartheta_{\mathrm{s}}(\zeta,\tau)$.
- At the inlet of the cathode gas channel: molar fractions $\chi_{i,\mathrm{m}}(\tau)$, temperatures $\vartheta_{\mathrm{m}}(\tau)$, and molar flow density $\gamma_{\mathrm{m}}(\tau)$.
  Abbreviation: $w_{\mathrm{m}}(\tau) := ((\chi_{i,\mathrm{m}})_{i\in\mathcal{I}}, \vartheta_{\mathrm{m}})$
- Potentials $\Phi_{\mathrm{a}}^{\mathrm{L}}(\zeta,\tau)$, $\Phi_{\mathrm{c}}^{\mathrm{L}}(\zeta,\tau)$, cell voltage $U_{\mathrm{cell}}(\tau)$.
  Abbreviation: $\Phi_{\mathrm{a|c}}^{\mathrm{L}} := (\Phi_{\mathrm{a}}^{\mathrm{L}}, \Phi_{\mathrm{c}}^{\mathrm{L}})$.
- I_{a}, I_{c} current produced by the electrochemical reaction at the anode resp. cathode, I_{e} current through the electrolyte.

Partial differential-algebraic equations with boundary conditions:

$$\frac{\partial \vartheta_{\mathrm{s}}}{\partial \tau} = c_1 \frac{\partial^2 \vartheta_{\mathrm{s}}}{\partial \zeta_1^2} + c_2 \frac{\partial^2 \vartheta_{\mathrm{s}}}{\partial \zeta_2^2} + \psi_1(\vartheta_{\mathrm{s}}, w_{\mathrm{a|c}}, \varphi_{\mathrm{a|c}}, \Phi_{\mathrm{a|c}}^{\mathrm{L}}, U_{\mathrm{cell}}),\ \frac{\partial \vartheta_{\mathrm{s}}}{\partial z}|_{\partial\Omega} = 0, \tag{1}$$

$$\frac{\partial w_{\mathrm{a}}}{\partial \tau} = -\gamma_{\mathrm{a}}\vartheta_{\mathrm{a}} \frac{\partial w_{\mathrm{a}}}{\partial \zeta_1} + \psi_2(\vartheta_{\mathrm{s}}, w_{\mathrm{a}}, \varphi_{\mathrm{a}}, \Phi_{\mathrm{a}}^{\mathrm{L}}), \quad w_{\mathrm{a}}|_{\partial\Omega_{\mathrm{a,in}}} = w_{\mathrm{a,in}}(\tau), \tag{2}$$

$$\frac{\partial w_{\mathrm{c}}}{\partial \tau} = -\gamma_{\mathrm{c}}\vartheta_{\mathrm{c}} \frac{\partial w_{\mathrm{c}}}{\partial \zeta_2} + \psi_3(\vartheta_{\mathrm{s}}, w_{\mathrm{c}}, \varphi_{\mathrm{c}}, \Phi_{\mathrm{c}}^{\mathrm{L}}, U_{\mathrm{cell}}), \quad w_{\mathrm{c}}|_{\partial\Omega_{\mathrm{c,in}}} = w_{\mathrm{m}}(\tau), \tag{3}$$

$$0 = -\frac{\partial(\gamma_{\mathrm{a}}\vartheta_{\mathrm{a}})}{\partial \zeta_1} + \psi_4(\vartheta_{\mathrm{s}}, w_{\mathrm{a}}, \varphi_{\mathrm{a}}, \Phi_{\mathrm{a}}^{\mathrm{L}}), \quad \gamma_{\mathrm{a}}|_{\partial\Omega_{\mathrm{a,in}}} = \gamma_{\mathrm{a,in}}(\tau), \tag{4}$$

$$0 = -\frac{\partial(\gamma_{\mathrm{c}}\vartheta_{\mathrm{c}})}{\partial \zeta_2} + \psi_5(\vartheta_{\mathrm{s}}, w_{\mathrm{c}}, \varphi_{\mathrm{c}}, \Phi_{\mathrm{c}}^{\mathrm{L}}, U_{\mathrm{cell}}), \quad \gamma_{\mathrm{c}}|_{\partial\Omega_{\mathrm{c,in}}} = \gamma_{\mathrm{m}}(\tau), \tag{5}$$

$$0 = \psi_6(\vartheta_{\mathrm{s}}, \chi_{\mathrm{a}}, \varphi_{\mathrm{a}}, \Phi_{\mathrm{a}}^{\mathrm{L}}), \quad 0 = \psi_7(\vartheta_{\mathrm{s}}, \chi_{\mathrm{c}}, \varphi_{\mathrm{c}}, \Phi_{\mathrm{c}}^{\mathrm{L}}, U_{\mathrm{cell}}), \tag{6}$$

$$\frac{\partial \Phi_{\mathrm{a|c}}^{\mathrm{L}}}{\partial \tau} = \psi_8(\vartheta_{\mathrm{s}}, \varphi_{\mathrm{a|c}}, \Phi_{\mathrm{a|c}}^{\mathrm{L}}, U_{\mathrm{cell}}, I_{\mathrm{a|e|c}}; I_{\mathrm{cell}}). \tag{7}$$

Integro differential-algebraic equations:

$$\frac{\mathrm{d}U_{\mathrm{cell}}}{\mathrm{d}\tau} = \frac{I_{\mathrm{a}} - I_{\mathrm{cell}}}{c_{\mathrm{a}}} + \frac{I_{\mathrm{e}} - I_{\mathrm{cell}}}{c_{\mathrm{e}}} + \frac{I_{\mathrm{c}} - I_{\mathrm{cell}}}{c_{\mathrm{c}}}, \tag{8}$$

$$I_{\mathrm{a}}(\tau) = \iint_{\Omega} i_{\mathrm{a}}(\vartheta_{\mathrm{s}}, w_{\mathrm{a}}, \varphi_{\mathrm{a}}, \Phi_{\mathrm{a}}^{\mathrm{L}})\,\mathrm{d}\zeta, \tag{9}$$

$$I_{\mathrm{c}}(\tau) = \iint_{\Omega} i_{\mathrm{c}}(\vartheta_{\mathrm{s}}, w_{\mathrm{c}}, \varphi_{\mathrm{c}}, \Phi_{\mathrm{c}}^{\mathrm{L}}, U_{\mathrm{cell}})\,\mathrm{d}\zeta, \tag{10}$$

$$I_{\mathrm{e}}(\tau) = \iint_{\Omega} i_{\mathrm{e}}(\Phi_{\mathrm{a|c}}^{\mathrm{L}})\,\mathrm{d}\zeta, \tag{11}$$

$$\frac{\mathrm{d}w_\mathrm{m}}{\mathrm{d}\tau} = \psi_9(w_\mathrm{m}, \int_{\partial\Omega_{\mathrm{a,out}}} w_\mathrm{a}\,\mathrm{d}\zeta_2, \int_{\partial\Omega_{\mathrm{a,out}}} \gamma_\mathrm{a}\,\mathrm{d}\zeta_2, \int_{\partial\Omega_{\mathrm{c,out}}} w_\mathrm{c}\,\mathrm{d}\zeta_1, \int_{\partial\Omega_{\mathrm{c,out}}} \gamma_\mathrm{c}\,\mathrm{d}\zeta_1, \lambda_\mathrm{air}, \vartheta_\mathrm{air}, R_\mathrm{back}), \tag{12}$$

$$\gamma_\mathrm{m}(\tau) = \psi_{10}(w_\mathrm{m}, \int_{\partial\Omega_{\mathrm{a,out}}} w_\mathrm{a}\,\mathrm{d}\zeta_2, \int_{\partial\Omega_{\mathrm{a,out}}} \gamma_\mathrm{a}\,\mathrm{d}\zeta_2, \int_{\partial\Omega_{\mathrm{c,out}}} w_\mathrm{c}\,\mathrm{d}\zeta_1, \int_{\partial\Omega_{\mathrm{c,out}}} \gamma_\mathrm{c}\,\mathrm{d}\zeta_1, \lambda_\mathrm{air}, \vartheta_\mathrm{air}, R_\mathrm{back}). \tag{13}$$

Initial conditions:

$$\begin{gathered}\vartheta_\mathrm{s}|_{\tau=0} = \vartheta_{0,\mathrm{s}}(\zeta),\ w_\mathrm{a}|_{\tau=0} = w_{0,\mathrm{a}}(\zeta),\ w_\mathrm{c}|_{\tau=0} = w_{0,\mathrm{c}}(\zeta),\ w_\mathrm{m}|_{\tau=0} = w_{0,\mathrm{m}},\\ \Phi^\mathrm{L}_\mathrm{a}|_{\tau=0} = \Phi^\mathrm{L}_{0,\mathrm{a}}(\zeta),\ \Phi^\mathrm{L}_\mathrm{c}|_{\tau=0} = \Phi^\mathrm{L}_{0,\mathrm{c}}(\zeta),\ U_\mathrm{cell}|_{\tau=0} = U_{0,\mathrm{cell}}.\end{gathered} \tag{14}$$

The formulae for ψ_k and the values of the positive constants $c_{\mathrm{a|e|c|1|2}}$ can be found in [1, 2] or [3], see also [7].

1.2 Discretized differential-algebraic equation system

Applying the method of lines (MOL) and a quadrature formula on (1–14) yields a semi-explicit differential-algebraic equation system of (perturbation=differential) index one in the new huge dimensional variable Y and diagonal matrix $M = \mathrm{diag}(E, O)$, E=identity matrix, O=zero matrix, cf. Sternberg [3],

$$M\dot{Y}(\tau) = \tilde{\psi}(Y(\tau), u(\tau), p), \qquad 0 = M[Y(0) - Y_0]. \tag{15}$$

The vector $u(\tau)$ denotes some or all of the input functions, e.g. $\gamma_{\mathrm{a,in}}(\tau)$, which can be used for (optimal) control purposes. The vector p denotes (some interesting) constants of the model, which will be perturbed in Sect. 3.

2 Fast load changes for an MCFC by optimal control

One drawback of molten carbonate fuel cells is the slow system reaction for load changes. The HotModule is operated in galvanostatic mode. A load change is modeled by a step-function in the cell current I_cell during the operation of the MCFC. In praxis a load change is usually realised by successively reducing the cell current by small steps to avoid material stresses caused by high temperature fluctuations inside the cell. Each step takes usually several hours to level out to a new stationary state of the MCFC. In this paper we focus on a single step to reduce the cell current. The following technologically interesting scenario is analysed (see [3], also for further scenarios):

At $\tau \le 0$ the computation is started with the stationary solution for constant $I_{\mathrm{cell},1} = 0.7$. The input variable cell current is prescribed as a discontinuous step function

$$I_\mathrm{cell}(\tau) = \begin{cases} I_{\mathrm{cell},1} = 0.7 & \text{if} \quad \tau \le 0, \\ I_{\mathrm{cell},2} = 0.6 & \text{if} \quad \tau > 0, \end{cases} \tag{16}$$

to model a load change for the MCFC.

A numerical simulation with constant boundary conditions at the anode inlet is compared with an optimally controlled molar flow densitiy $\gamma_{\mathrm{a,in}}(\tau)$ at the anode inlet (see Fig. 3). Goal of the optimal control is to reach faster the new stationary state after the load change at time $\tau = 0$.

The cell voltage U_cell reacts very fast and significantly on a sudden load change of the cell current (Fig. 2) and reacts also on changes of the slowest variable, the solid temperature ϑ_s. A constant cell voltage U_cell indicates that the (new) stationary state has been reached. Therefore the tracking type cost functional

$$\min \int_0^{\tau_\mathrm{f}} \left[U_\mathrm{cell}(\tau) - U_{\mathrm{cell,2,stationary}}\right]^2 \mathrm{d}\tau \quad \text{with} \quad U_{\mathrm{cell,2,stationary}} = 30.788 \tag{17}$$

is used for optimal control purposes.

Hereby one searches for an optimal control function

$$u(\tau) = \gamma_{\mathrm{a,in}}(\tau) \in [0.85, 1.5] \tag{18}$$

such that the initial value problem (15), i.e. the discretized version of Eqs. (1–14), is fulfilled, and the cost functional (17) is minimized.

Since the solution of this problem is too time consuming, a slightly modified variant is solved numerically. A sequence of $k = 1, \ldots, 5$ optimal control problems with cost functionals

$$\min \int_{\tau_k}^{\tau_{k+1}} \left[U_{\mathrm{cell}}(\tau) - U_{\mathrm{cell,2,stationary}}\right]^2 \mathrm{d}\tau \tag{19}$$

and constraints (15, 18) is solved. A quasi-logarithmic type grid $\tau_1 = 0$, $\tau_2 = 0.1$, $\tau_3 = 1.1$, $\tau_4 = 11.1$, $\tau_5 = 111.1$, $\tau_6 = \tau_{\mathrm{f}} = 1111.1$ is used, due to the different time scales of the state variables. The electrical variables are very fast, the solid temperature is very slow, all other states are moderately fast. In each subintervall $[\tau_k, \tau_{k+1}]$ the control is discretized on an equidistant subgrid. Initial conditions for the first optimal control problem are the stationary solution for $I_{\mathrm{cell},1}$. Initial conditions for the $(k+1)$-th optimal control problem
Fig2 are the free final conditions of the k-th optimal control problem.

Fig. 2 and 3 present the cell voltage $U_{\mathrm{cell}}(\tau)$ and the optimal control $\gamma_{\mathrm{a,in}}(\tau)$ in the five time subintervals $[\tau_k, \tau_{k+1}]$. In each subinterval a linear time scale is depicted in the figures.

A fast increase of the cell voltage can be seen in the simulation until $\tau \approx 0.005$. (One unit of the dimensionless time τ equals 12.5 seconds.) This is the immediate consequence of the very fast change of the electrical variables. A moderate increase until $\tau \approx 0.015$ is due to the fast change of the molar quantities. The final stationary value is reached only after about $\tau \approx 1000$ (more than 3 hours) due to the slow changes in the solid temperature ϑ_{s}. The oscillating behavior while reaching the new stationary cell voltage has undesirable effects on the cell power $P_{\mathrm{cell}} = I_{\mathrm{cell}}\, U_{\mathrm{cell}}$ and should be avoided.

In contrast the new stationary cell voltage $U_{\mathrm{cell,2,stationary}}(\tau)$ is reached significantly
Fig3 earlier for optimally controlled boundary conditions $\gamma_{\mathrm{a,in}}(\tau)$ at the anode inlet.
Fig4

3 Sensitivity analysis of the optimal solution

Starting from the preceding optimal load change we are interested in the dynamical behaviour of the computed optimal solution if some of the (model) parameters are varying. They are collected in a parameter vector p=(p_1, p_2, p_3).

Under certain regularity assumptions, the *optimal* state $Y_{\mathrm{opt}}(\tau, p)$ and the *optimal* control $u_{\mathrm{opt}}(\tau, p)$ of (15, 18, 19) depend continuously directional differentiable on the parameter vector p, such that first order approximations

$$Y_{\mathrm{opt}}(\tau, p) \approx Y_{\mathrm{opt}}(\tau, p_o) + \frac{\partial Y_{\mathrm{opt}}}{\partial p}(\tau, p_o)(p - p_o), \tag{20}$$

$$u_{\mathrm{opt}}(\tau, p) \approx u_{\mathrm{opt}}(\tau, p_o) + \frac{\partial u_{\mathrm{opt}}}{\partial p}(\tau, p_o)(p - p_o) \tag{21}$$

with respect to a reference parameter value p_o=0 are valid (cf. Büskens and Maurer [8]). See Fig. 4–12 and the following discussion for the results of the MCFC model. The optimal control software NUDOCCCS (Büskens [9]) is used to compute numerically both the optimal solution and the sensitivity differentials $\frac{\partial Y_{\mathrm{opt}}}{\partial p}(\tau, p_o)$, $\frac{\partial u_{\mathrm{opt}}}{\partial p}(\tau, p_o)$ of (20, 21) by a direct solution approach [8, 9] which transforms the optimal control problem into a nonlinear programming problem. The nonlinear programming problem is solved by an SQP algorithm. The sensitivities are computed using the Karush-Kuhn-Tucker equations [10] and data already provided by the SQP algorithm.

Therefore the solution of *one* optimal control problem for a reference parameter p_o and an a posteriori computation of the sensitivity differentials can replace the usual engineering approach of solving a large number of optimal control problems (15, 18, 19) for *a family* of interesting parameter values p.

We investigate the sensitivities beginning with the cell current $I_{\mathrm{cell},2}$, that directly influences all states in the MCFC model. Subsequently we present the sensitivities with respect

to the anode inlet temperature $\vartheta_{\mathrm{a,in}}$, that primarily affects the variables in the anode gas channel, and finally with respect to the air number λ_{air}, that basically influences the states in the burner, in the mixer and consequently the states in the cathode gas channel.

The reactions of the states can be arranged into three groups according to their time constants. Exemplarily we present the sensitivity of the slow changing solid temperature ϑ_{s} and of the very fast adapting cell voltage U_{cell}. Moreover we are interested in the robustness of the computed optimal control.

3.1 Sensitivity analysis of a perturbation in the cell current

First, we consider a perturbation p_1 in the new cell current $I_{\mathrm{cell},2} = 0.6 + p_1$, see (16). The sensitivity $\frac{\partial \vartheta_{\mathrm{s}}}{\partial p_1}$ of the solid temperature with respect to the perturbation is shown in Fig. 5. Starting from zero, because the initial conditions are unchanged, the sensitivity increases uniformly distributed along the flow direction ζ_2 with time τ. This yields a higher but still steady temperature distribution in the solid. As a consequence the material is stressed by higher temperatures but not by higher temperature gradients.

The cell voltage U_{cell} adapts very fast to the new cell voltage $U_{\mathrm{cell,2,stationary}}$. The way how it adapts is strongly influenced by the cell current. As shown in Fig. 6 there are high sensitivities in the first seconds. The optimal control is then able to level out to the given nominal value. The sensitivity $\frac{\partial U_{\mathrm{cell}}}{\partial p_1}$ drops to zero for large times.

The optimal controls $\gamma_{\mathrm{a,in}}(\tau, p_1)$ for $p_1 = 0$ and $p_1 = 0.01$ differ due to their different stationary states. Therefore the sensitivity $\frac{\partial \gamma_{\mathrm{a,in}}}{\partial p_1}$ of the optimal control does not vanish for all times, see Fig. 7–8. Some peaks of the sensitivity $\frac{\partial \gamma_{\mathrm{a,in}}}{\partial p_1}$ are due to the parameter dependency of exit and entry times on the boundary of the admissible set for the optimal control. Fig5 Fig6 Fig7 Fig8

3.2 Sensitivity analysis of a perturbation in the anode inlet temperature

In the second case we consider a perturbation p_2 in the anode inlet temperature $\vartheta_{\mathrm{a,in}} = 3.0 + p_2$. Compared to the perturbed cell current, Fig. 9 shows only a very small sensitivity of the solid temperature.

The cell voltage and the optimal control (Fig. 4) show significant sensitivities only in the the first seconds, that is to say close to the exit and entry point of the control constraint (cf. [3]). Fig9

3.3 Sensitivity analysis of a perturbation in the air number

In the third case we investigate a perturbation of the air number $\lambda_{\mathrm{air}} = 2.3 + p_3$ at the air inlet of the catalytic burner. Fig10

The variables in the cathode gas channel are directly affected by the perturbed air number. The cathode gas temperature ϑ_{c} for example shows a high sensitivity. The change in the cathode gas temperature influences the solid temperature ϑ_{s} via heat conduction. Thus, Fig. 10 shows a significant sensitivity of the solid temperature ϑ_{s}.

Driven by the fast changes in the cathode gas channel, the cell voltage U_{cell} increases as indicated by its positive sensitivity in Fig. 11. The control has to make sure that the desired cell voltage $U_{\mathrm{cell,2,stationary}}$ is reached despite of the perturbations. The sensitivity of the optimal control is depicted in Fig. 12. Since the sensitivity differs from zero for large times, the optimal control of the perturbed system differs also for large times from the reference system. Fig11 Fig12

4 Conclusion

Complicated dynamical systems are often modeled by large PDE/PDAE systems. Parameters of these models are often estimated or measured from experiments and may contain

errors or may vary. These perturbations may lead to differences between the simulation results and the real system and are to be avoided. Hence, when these models are taken for simulation and optimal control, the results must be analyzed concerning perturbations in those parameters.

In this paper we have presented the optimal control of a MCFC model for load changes. The molar flow density at the anode inlet is controlled in order to ensure a fast and stable load change. The results are tested for perturbations in three input parameters. Our investigations show that the system reacts relatively sensitive to perturbations in the cell current: Electric variables affect the whole MCFC system. In contrast, the influence of the gas temperature at the anode inlet to the solid temperature and the cell voltage of the MCFC is of lower order: The gas temperature in the anode channel is dominated by heat exchange due to chemical reactions (endothermic internal reforming, exothermic oxidation). However, there are other quantities controlling the gas flows that have more influence on the dynamical behaviour of the MCFC, e.g. the air number at the air inlet of the catalytic burner. Perturbations in the air number effect the composition and temperature of the cathode gas and significantly influence the cell behaviour via heat and ion conduction.

Perturbation in electrical variables like the cell current have an influence on the whole fuel cell. In contrast, variables associated with the gas flows may have primarily local influence like the anode inlet temperature or may have global influence like the air number.

All sensitivity studies have one common result: The structure of the optimal control remains unchanged. At first the gas flow is maximal until the new stationary cell voltage is reached for the first time. After a period of minimal gas flow, the gas flow tends to its new stationary value.

Since the switching structure of the optimal control is stable with respect to perturbations and since the optimal value of the cost functional varies only in the order of the perturbations, the MCFC model is robust and adequate for optimal control; see [3] too.

The computation of the optimal solution for a scalar control takes 2 CPU hours (with more control variables up to 48 CPU hours). If the computation of the sensitivity differentials is included approximately 70 CPU hours are needed.

In practical operation of fuel cell systems the assumption of perfectly stationary states is not valid. In order to react to fluctations and deviations from perfectly stationary states, it may be helpful to compute sensitivities with respect to the initial values in an analogous way.

Future investigations will be devoted to proper orthogonal decomposition (POD) techniques in order to decrease computing time.

Acknowledgements

This research was partly funded by the German Federal Ministry of Education and Research (BMBF) within the WING-project "Optimierte Prozessführung von Brennstoffzellensystemen mit Methoden der Nichtlinearen Dynamik". The first author was funded by the *Promotionsabschlussstipendium des HWP-Programms "Chancengleichheit für Frauen in Forschung und Lehre"*.

We are indebted to our BMBF project partners Dr.-Ing. P. Heidebrecht and Prof. Dr.-Ing. K. Sundmacher from the Max-Planck-Institut für Dynamik komplexer technischer Systeme Magdeburg for providing us with the complicated fuel cell model and to Dipl.-Ing. J. Berndt and Dipl.-Ing. M. Koch from the management of IPF Heizkraftwerksbetriebsges. mbH Magdeburg for their continual support.

We are indebted to Prof. Dr. C. Büskens from University of Bremen for providing us with the direct optimal control software package NUDOCCCS.

List of abbreviations

DAE	Differential-algebraic equation system
MCFC	Molten carbonate fuel cell
MOL	Method of lines
PDAE	Partial differential-algebraic equation system
PDE	Partial differential equation (system)
2D	Dimension of the independent spatial coordinate

List of indice

i	$\in \mathcal{I} = \{CH_4, H_2O, H_2, CO, CO_2, O_2, N_2\}$
j	compartment or layer in solid
a, c, e, m, s	anode, cathode, electrolyte, mixer, solid
in, out	inlet, outlet
air	boundary data at air inlet
0	initial data
o	nominal value
opt	optimal solution

List of symbols

c_a, c_e, c_c, c_1, c_2	positive constants
i_a, i_e, i_c	current density in different layers of the solid
p	perturbation vector
u	control (function)
w_j	$= (\chi_j, \vartheta_j)$
$w_{a\|c}$	$= (w_\mathrm{a}, w_\mathrm{c})$
I_a, I_e, I_c	current in different layers of the solid
I_cell	total cell current
P_cell	electric power
R_back	$\in [0,1]$, switch for cathode recycle
U_cell	cell voltage
Y	variables after MOL-discretization
γ	molar flow densitity
$\zeta = (\zeta_1, \zeta_2)$	spatial coordinates
ϑ	temperature
λ_air	air number
τ	time
φ	partial pressure
χ	molar fraction
ψ, $\tilde{\psi}$	nonlinear functions
$\Phi_\mathrm{a}^\mathrm{L}$, $\Phi_\mathrm{c}^\mathrm{L}$	electric potential at anode/cathode ion layer
$\Phi_\mathrm{a\|c}^\mathrm{L}$	$= (\Phi_\mathrm{a}^\mathrm{L}, \Phi_\mathrm{c}^\mathrm{L})$
Ω	$= [0,1] \times [0,1]$, spatial domain
$\partial\Omega$	boundary of spatial domain Ω
$\partial\Omega_\mathrm{a,in}$	anode inlet, $\zeta_1 = 0$
$\partial\Omega_\mathrm{c,in}$	cathode inlet, $\zeta_2 = 0$
$\partial\Omega_\mathrm{a,out}$	anode outlet, $\zeta_1 = 1$
$\partial\Omega_\mathrm{c,out}$	cathode outlet, $\zeta_2 = 1$

References

1. Heidebrecht, P., 2005, "Modelling, Analysis and Optimisation of a Molten Carbonate Fuel Cell with Direct Internal Reforming (DIR-MCFC)," VDI Fortschritt Berichte, Reihe 3, Nr. 826, VDI Verlag, Düsseldorf, Germany.

2. Heidebrecht, P., and Sundmacher, K., 2005, "Dynamic Model of a Cross-Flow Molten Carbonate Fuel Cell with Direct Internal Reforming," Journal of the Electrochemical Society, **1**52, pp. A2217–A2228.
3. Sternberg, K., 2007, "Simulation, Optimale Steuerung und Sensitivitätsanalyse einer Schmelzkarbonat-Brennstoffzelle mithilfe eines partiellen differential-algebraischen dynamischen Gleichungssystems," Dissertation, Universität Bayreuth, Bayreuth, Germany.
4. Pesch, H.J., Sternberg, K., and Chudej, K., 2006, "Towards the Numerical Solution of a Large Scale PDAE Constrained Optimization Problem Arising in Molten Carbonate Fuel Cell Modeling," In: G. Di Pillo, M. Roma (Eds.): Large Scale Nonlinear Optimization. Springer, New York, pp. 243–253.
5. Bischoff, M., and Huppmann, G., 2002, "Operating experience with a 250 kW_{el} molten carbonate fuel cell (MCFC) power plant," Journal of Power Sources, **105** (2), pp. 216–221.
6. Gundermann, M., Heidebrecht, P., and Sundmacher, K., 2006, "Validation of a Mathematical Model Using an Industrial MCFC Plant," Journal of Fuel Cell Science and Technology **3**, pp. 303–307.
7. Sundmacher, K., Kienle, A., Pesch, H.J., Berndt, J.F., and Huppmann, G., (Eds.), 2007, "Molten Carbonate Fuel Cells – Modeling, Analysis, Simulation, and Control," Wiley-VCH, Weinheim.
8. Büskens, C., and Maurer, H., 2001, "Sensitivity Analysis and Real-Time Control of Parametric Optimal Control Problems Using Nonlinear Programming Methods," In: M. Grötschel, S.O. Krumke, J. Rambau (Eds.): Online Optimization of Large Scale Systems, Springer, Berlin, pp. 57–68.
9. Büskens, C., 1998, "Optimierungsmethoden und Sensitivitätsanalyse für optimale Steuerprozesse mit Steuer- und Zustands-Beschränkungen," Dissertation, Universität Münster, Münster, Germany.
10. Büskens, C., and Maurer, H., 2001, "Sensitivity Analysis and Real-Time Control of NLP Problems," In: M. Grötschel, S.O. Krumke, J. Rambau (Eds.): Online Optimization of Large Scale Systems, Springer, Berlin, pp. 3–16.

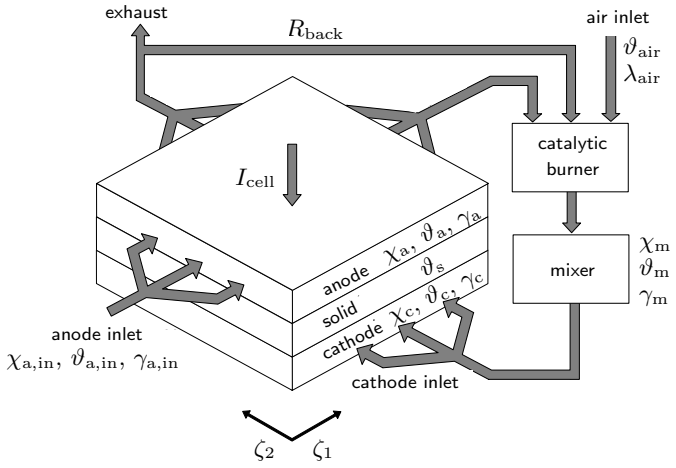

Fig. 1. 2D MCFC crossflow model with compartments and mathematical variables

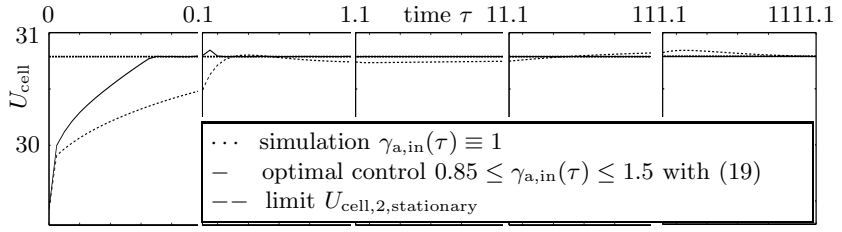

Fig. 2. Simulated and optimal controlled cell voltage U_{cell} of MCFC model

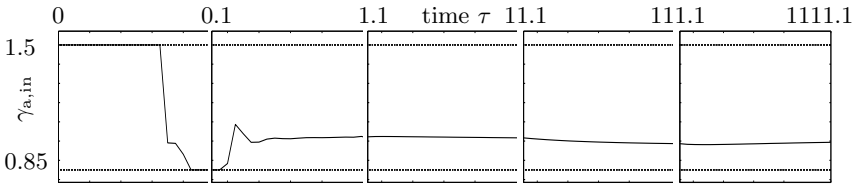

Fig. 3. Optimal control molar flow density $\gamma_{\text{a,in}}(\tau)$ at anode inlet (without perturbation)

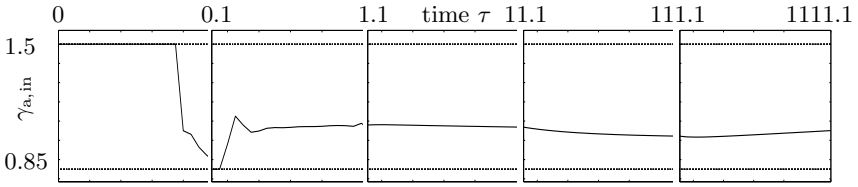

Fig. 4. Optimal control molar flow density $\gamma_{\text{a,in}}(\tau)$ at anode inlet with perturbation $p_2 = 0.01$ in anode inlet temperature $\vartheta_{\text{a,in}} = 3.0 + p_2$

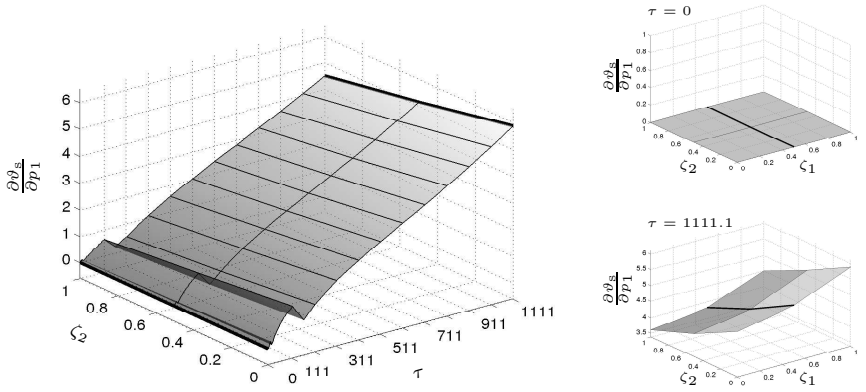

Fig. 5. Sensitivity $\frac{\partial \vartheta_s}{\partial p_1}$ in $\zeta_1 = 0.5$ with respect to a perturbation in the cell current I_{cell}

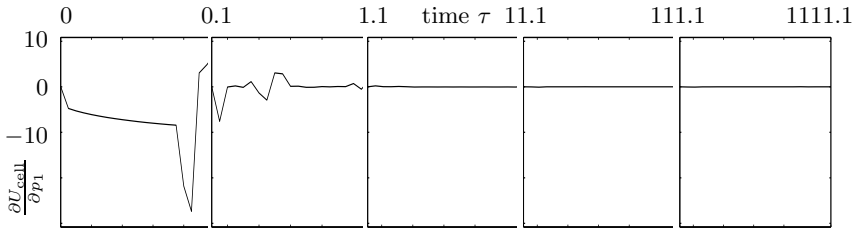

Fig. 6. Sensitivity $\frac{\partial U_{\text{cell}}}{\partial p_1}$ with respect to a perturbation in the cell current I_{cell}

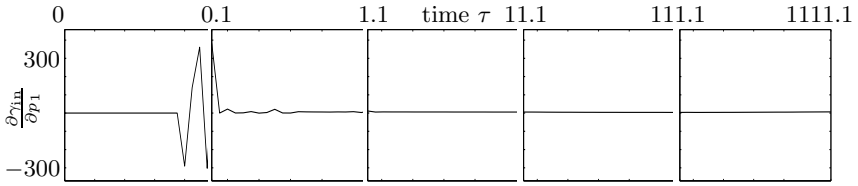

Fig. 7. Sensitivity $\frac{\partial \gamma_{\text{a,in}}}{\partial p_1}$ with respect to a perturbation in the cell current I_{cell}

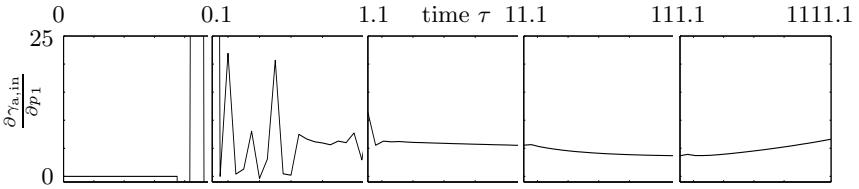

Fig. 8. Sensitivity $\frac{\partial \gamma_{\text{a,in}}}{\partial p_1}$ (scaled axis) with respect to a perturbation in the cell current I_{cell}

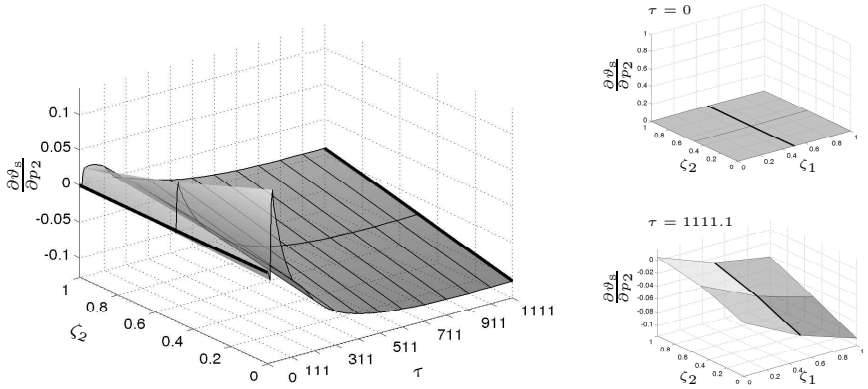

Fig. 9. Sensitivity $\frac{\partial \vartheta_s}{\partial p_2}$ in $\zeta_1 = 0.5$ with respect to a perturbation in the anode inlet temperature $\vartheta_{\text{a,in}}$

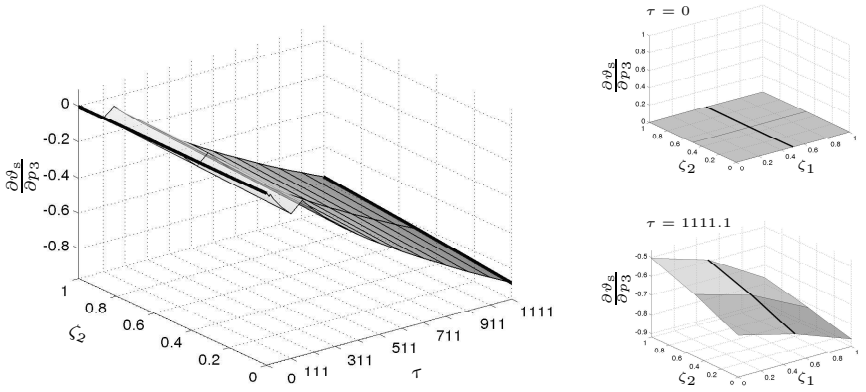

Fig. 10. Sensitivity $\frac{\partial \vartheta_s}{\partial p_3}$ in $\zeta_1 = 0.5$ with respect to a perturbation of the air number $\lambda_{\text{air}} = 2.3 + p_3$

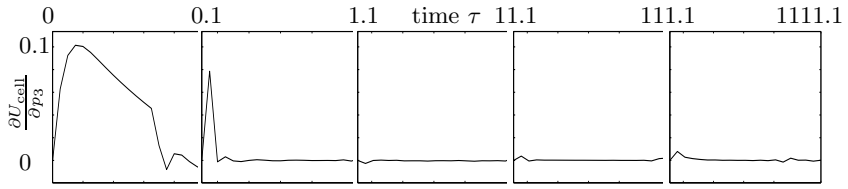

Fig. 11. Sensitivity $\frac{\partial U_{\text{cell}}}{\partial p_3}$ with respect to a perturbation in $\lambda_{\text{air}} = 2.3 + p_3$

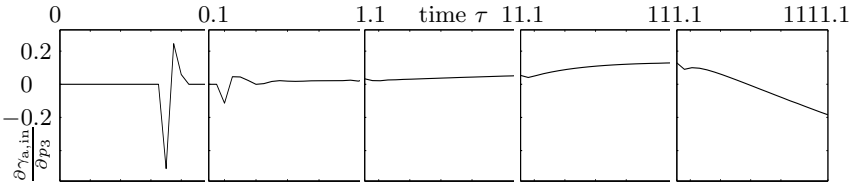

Fig. 12. Sensitivity $\frac{\partial \gamma_{\text{a,in}}}{\partial p_3}$ with respect to a perturbation in $\lambda_{\text{air}} = 2.3 + p_3$